International Journal of Engineering & Technology, 7 (4.20) (2018) 601-606

International Journal of Engineering & Technology

Website: www.sciencepubco.com/index.php/IJET

Research paper

Land Surface Temperature Retrieval from LANDSAT-8 Thermal Infrared Sensor Data and Validation with Infrared Thermometer Camera

Muhammad Mejbel Salih[1], Oday Zakariya Jasim[1], Khalid I. Hassoon[2], Aysar Jameel Abdalkadhum[3]*

[1] *Civil Engineering Department, University of Technology*
[2] *Ministry of Science and Technology*
[3]*College of Water Resources Engineering, Al-Qasim Qreen University*
**Corresponding author E-mail: Aysar@wrec.uoqasim.edu.iq*

Abstract

This paper illustrates a proposed method for the retrieval of land surface temperature (LST) from the two thermal bands of the LANDSAT-8 data. LANDSAT-8, the latest satellite from Landsat series, launched on 11 February 2013, using LANDSAT-8 Operational Line Imager and Thermal Infrared Sensor (OLI & TIRS) satellite data. LANDSAT-8 medium spatial resolution multispectral imagery presents particular interest in extracting land cover, because of the fine spectral resolution, the radiometric quantization of 12 bits. In this search a trial has been made to estimate LST over Al-Hashimiya district, south of Babylon province, middle of Iraq. Two dates images acquired on 2nd &18th of March 2018 to retrieve LST and compare them with ground truth data from infrared thermometer camera (all the measurements contacted with target by using type-k thermocouple) at the same time of images capture. The results showed that the rivers had a higher LST which is different to the other land cover types, of less than 3.47 C ◦, and the LST different for vegetation and residential area were less than 0.4 C ◦ with correlation coefficient of the two bands 10 and 11 R_{bnad10}= 0.70, R_{band11} = 0.89 respectively, for the imaged acquired on the 2nd of march 2018 and R_{band10}= 0.70 and R_{band11} = 0.72 on the 18th of march 2018. These results confirm that the proposed approach is effective for the retrieval of LST from the LANDSAT-8 Thermal bands, and the IR thermometer camera data which is an effective way to validate and improve the performance of LST retrieval. Generally the results show that the closer measurement taken from the scene center time, a better quality to classify the land cover. The purpose of this study is to assess the use of LANDSAT-8 data to specify temperature differences in land cover and compare the relationship between land surface temperature and land cover types.

Keywords: *land cover type; Land surface temperature (LST); LANDSAT-8 thermal bands; IR thermometer camera (thermocouple).*

1. Introduction

Land surface temperature (LST) play an important role in research on agricultural analyses, effects of urban heat island, and environmental monitoring [1]. However, significant advancement has been made in these applications with a series of remote sensing satellites being launched [1-4]. LST divergences in space and time, measured by satellite remote sensing data, were used for the assessment of a lot of geophysical variables, such as soil moisture, vegetation water stress, evapotranspiration, and thermal inertia [5-7]. With a view to accurately retrieve LST, methods have been continuously developed, they can be roughly gather into three groups: the single-channel algorithm [8], multi-channel algorithm [9-15], and multi-angle algorithm [16]. In general, using multi-channel algorithm is the split-window algorithm that takes the interest of atmospheric water vapor absorption difference between two channels centered at 11.0 µm and 12 µm to remove the effectiveness of atmosphere [9]. In recent decades, a series of sensors which have been sent into space, such as the Moderate-resolution Imaging Spectroradiometer (MODIS) aboard Terra and Aqua, Advanced Very High Resolution Radiometer (AVHRR) on series of National Oceanic and Atmospheric Administration (NOAA) satellite, have provided public range global thermal data twice daily, using two long wave infrared (LWIR) bands [17]. Thematic Mapper (TM) and Enhanced Thematic Mapper Plus (ETM+) aboard previous LANDSAT-5 and LANDSAT-7 satellites provide thermal data using only one (LWIR) band, with higher spatial resolution within 16-days temporal resolution. LANDSAT-8 was successfully launched on the 11th of February 2013 into space with two instrument on board, the Operational Land Imager (OLI) and the Thermal Infrared Sensor (TIRS) [18]. The OLI instrument with nine spectral bands in the visible (VIS), near infrared (NIR) (Table 1), and the shortwave infrared (SWIR) spectral regions, while the TIRS instrument with two thermal infrared spectral bands in the LWIR respectively centered at 10.9 µm and 12 µm (Table 2). The relative spectral response of both OLI and TIRS channels are illustrated in Fig 1. Further, another advantage is that the OLI, and TIRS instruments observed Earth's surface with resolution from 15 meters to 100 meters. According to the technical specification, the LANDSAT-8 are very suitable for retriever LST. Therefore, the objective of this paper is to retrieve LST and compare them with trained and validated ground truth data from infrared thermometer camera (IR thermometer) at the same time the images were acquired.

Copyright © 2018 Authors. This is an open access article distributed under the Creative Commons Attribution License, which permits unrestricted use, distribution, and reproduction in any medium, provided the original work is properly cited.

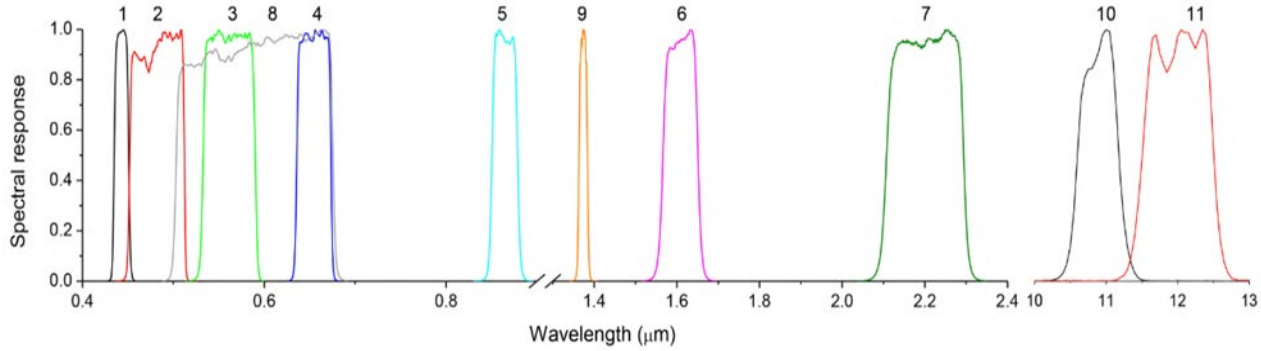

Fig. 1: Spectral response of OLI and TIRS channels [19]

Table 1: Technical specification of operational image (OLI) on LANDSAT-8[18]

Band Name	Spectral range (μm)	Spatial resolution (m)
Band 1 Visible Ultra Blue (Coastal)	0.435-0.451	30
Band 2 Visible (Blue)	0.452-0.512	30
Band 3 Visible (Green)	0.533-0.590	30
Band 4 (Red)	0.636-0.673	30
Band 5 Near-Infrared (NIR)	0.851-0.879	30
Band 6 Shortwave Infrared (SWIR 1)	1.566-1.651	30
Band 7 Shortwave Infrared (SWIR 2)	2.107-2.294	30
Band 8 Panchromatic (Pan)	0.503-0.676	15
Band 9 (Cirrus)	1.363-1.384	30

Table 2: Technical specification of thermal infrared sensor (TIRS) on LANDSAT-8[18].

Band Name	Central wavelength (μm)	Spectral range (μm)	Spatial resolution (m)
Band 10 TIRS 1	10.9	10.6 – 11.19	100 (30)*
Band 11 TIRS 2	12.0	11.5 – 12.51	100(30)*

* TIRS bands are acquired at 100 meter resolution, but are resampled to 30 meter in delivered data product.

2. Study Area and Dataset

2.1. Study Area

Al-Hashimiya district is a part of Babil province, Iraq, which consist of four cities. It is located along the Shatt Al-Hashimiya, while the city of Al-Qassim is located to the south, and Al-Madhatiya and Al-Shomali cities are located to the east. Al-Hashimiya district occupies an area of 1836.74 square kilometers (183674.166 hectares) and it is located to the south of Babil province approximately between 44◦ 30` - 45◦ 15` E longitude and 32◦ 00` -32◦ 30` N latitudes. The population of the district is about 600, 000 people. It is characterized by its agricultural and rural areas and the moderate weather ranges between the maximum and minimum temperature (45◦- 4◦) C◦. The Date palm trees cover a wide are, up to more than 2 million trees. It is characterized by the cultivation of field crops, especially wheat, barley and corn, where the agricultural area is covered more than 123000 hectares, according to the statistics of the province of Babylon in 2017 .The Al-Hashimiya district is considered the geographical center of Iraq, where the distance from east to west of Iraq is equal to the distance from north to south.

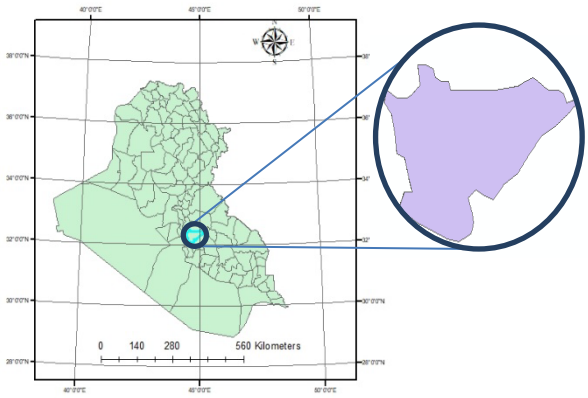

Fig. 2: Study area Al-Hashimiya district, Iraq

2.2 .Satellite Data

The multispectral remote sensing images of Al-Hashimiya city of two dates were collected from USGS website. LANDSAT-8 satellite images revisit earth once in 16 days. Bands descriptions of LANDSAT-8 are as given in table 1 and 2 (https://landsatlook.usgs.gov). Satellite data over Al-Hashimiya city of the 2nd and the 18th of March 2018 (day time, level-1TP product, path/raw 168/38) have been used in this study. Both were downloaded from USGS with image quality 9. The study area consist vegetation cover, bare soil, water and residential area. All the data were re-projected to a Universal Transverse Mercator (UTM) coordinate system, datum WGS84, zone 38.

2.3. Infrared Thermometer Camera (IR Thermometer)

Infrared thermometer measure the surface temperature of an opaque object [20]. The thermometer's optics sense emitted, reflected, and transmitted energy, which is gathered and centered onto a detector. The unit's electronics translate the information into a temperature reading which the displays on screen (see Figure 3). The Infrared Thermometer Camera as shown in figure (4-a) is for non-contact temperature measurement. This thermometer determines object's surface temperature by measuring the amount of infrared energy radiated by the object's surface [20]. The thermometer also support contact temperature measurement via K-type thermocouple as shown in figure (4-b). In this paper all the land surface temperature measurements (ground-truth) taken by using type-K (thermocouple). The main Specifications of the IR temperature camera is illustrated in Table 3. Field measurements were observed by using Infrared Thermometer. The observations were measured with direct connection with land surface at the same time of the acquisition of images. The meteorological data recorded the minimum and maximum temperature degree ranges 18 to 25 C◦ and 9 to 24 C◦ for the days 02/03/2018 and 18/03/2018 respectively.

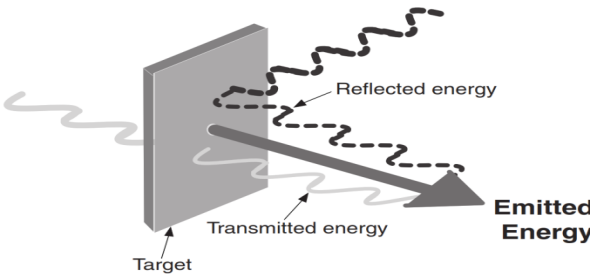

Fig.3: How the Thermometer Works [20].

Fig. 4: a-Infrared thermometer camera, b- K-type thermocouple [20].

Table 3: IR Thermometer measurement non-contact (infrared) temperature measurements [20]

Temperature range	-50 to 1000 C◦
Accuracy	1 C◦
Resolution	640*480 pixels
Display resolution	0.1 C◦ < 1000 C◦
Response time	150 ms
Spectral response	8~14 µm
Display resolution	Digitally corrected from 0.1 to 1.0
Type-k thermocouple measurements with connection with land surface	
Temperature range	-50 to 1370 C◦
Accuracy	0.5 C◦
Display resolution	0.1 C◦ < 1000 C◦ < 1000 C◦
Display resolution	Adjustable emissivity

3. Methodology

The algorithm of the proposed work to retrieve LST is shown in the Fig. 5. This approach can only use to process LANDSAT-8 data. In this paper, two bands 10 and 11 are used to estimate brightness temperature and the red band (4), near infrared band (5) are used to compute the Normalized Difference vegetation Index (NDVI).

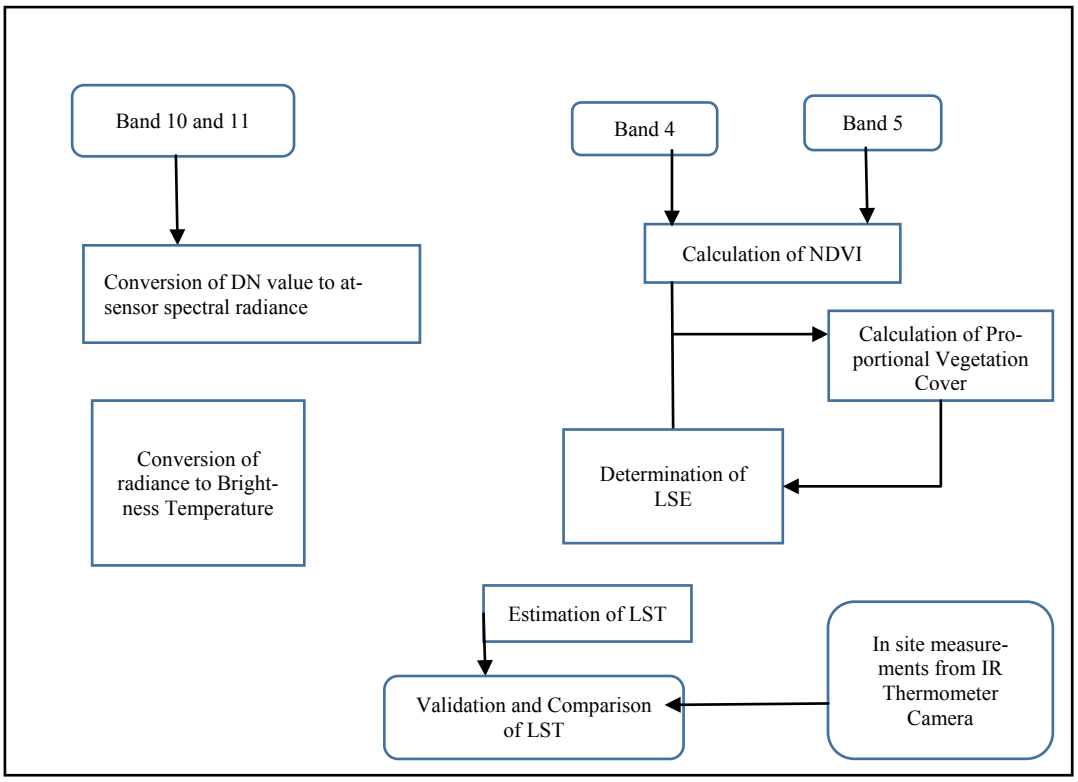

Fig. 5: Flow diagram for LST retrieval

The steps included in the proposed work are detailed in the following literature.

1- The LANDSAT-8 data products were geometrically corrected data set. The metadata of the satellite images is shown in the table 4.The first step of the proposed work is the satellite-based digital number (DN) is converted to at-sensor spectral radiance (Lλ) using the following equation [21]:

$$L_\lambda = M_L\, Q + A_L \quad (1)$$

Where M_L= Band specific multiplicative rescaling factor from the metadata, Qcal= Quantized and calibrated standard product DN value of pixel, and A_L= Band-specific additive rescaling factor from the metadata.

Table 4: Metadata oh the LANDSAT-8 satellite image.

Band	Variable	Description	Value
10		Thermal band	
	K_1	Thermal constant	774.8853
	K_2		1321.0789
	M_L	RADIANCE_MULT_BAND	0.000 33420
	Q_{cal}	DN value of pixel	
	A_L	RADIANCE_ADD_BAND	0.1
11		Thermal band	
	K1	Thermal constant	480.8883
	K2		1201.1442
	M_L	RADIANCE_MULT_BAND	0.000 33420
	Qcal	DN value of pixel	
	A_L	RADIANCE_ADD_BAND	0.1

2- The thermal infrared bands should be converted to brightness temperature (BT) using metadata and the following equation [21].

$$\mathbf{BT} = \frac{K_2}{\ln[(\frac{K_1}{L_\lambda})+1]} - 273.15 \quad (2)$$

Where K1 and K2 are the thermal infrared (TIRS) bands 10 and 11 which can be find in the metadata file linked with the satellite image. To have the results in Celsius (C◦) it is needed to refine by adding absolute zero which is approximately equal to – 273.15.

3- (NDVI) is necessary to identify land cover types of the area study. The NDVI ranges between -1 to +1. NDVI is computed on per-pixel basis as the normalized difference between the red band (0.636-0.673µm) and near infrared band (0.851-0.879µm) of images using following equation

$$\mathbf{NDVI} = \frac{(\mathbf{NIR}-\mathbf{RED})}{(\mathbf{NIR}+\mathbf{RED})} \quad (3)$$

Where NIR is the near infrared band value of pixel and RED is the red band of same pixel. The NDVI is essential to calculate proportional vegetation (Pv) and emissivity (ε).

4- From NDVI values obtained in the previous step calculate proportional vegetation (Pv). This proportional vegetation gives the estimation of area under each land cover type. The vegetation and bare soil proportions are acquired from the NDVI of pure pixel.

$$\mathbf{Pv} = (\frac{\mathbf{NDVI}-\mathbf{NDVI_s}}{\mathbf{NDVI_v}-\mathbf{NDVI_s}})^2 \quad (4)$$

5- Computation of land surface emissivity (LSE) is required to estimation LST. Land surface emissivity that is describes the radiative absorption ability of a surface in loge wave radiation spectrum [22]. LSE is largely dependent on the target surface top layer such as type of soil, surface roughness, and nature of vegetation cover [23]. To obtained LSE, the following equation using [23]:

$$\varepsilon = \varepsilon_{v\lambda}.\boldsymbol{P_V} + \varepsilon_{s\lambda}.(\mathbf{1}-\boldsymbol{P_V}) + \boldsymbol{C_\lambda} \quad (5)$$

Where ε = Land Surface Emissivity
$\varepsilon_{S\lambda}$= emissivity of soil
$\varepsilon_{V\lambda}$ = emissivity of vegetation
PV = proportion of vegetation
C_λ = surface roughness taken as a constant value of 0.009

The emissivity of water bodies is very settled in comparison with land surfaces. Since the emissivity depends on the wavelength, the NDVI can be used to estimate the emissivity of different land surfaces in the 10-12 µm range [22].

$$\varepsilon_\lambda = \begin{cases} \varepsilon_{S\lambda} & NDVI < NDVI_S \\ \varepsilon_{S\lambda}\, P_V + \varepsilon_{S\lambda}(1-P_V) + C_\lambda & NDVI_S \le NDVI \le NDVI_V \\ \varepsilon_{S\lambda} + C_\lambda & NDVI > NDVI_V \end{cases} \quad (6)$$

6- The final step is to calculate LST using brightness temperature (BT) of two bands 10, 11 and LSE that is derived from Pv and NDVI [23].LST can be retrieved using the following equation:

$$\mathbf{LST} = \frac{\boldsymbol{BT}}{[\mathbf{1}+\{(\frac{\lambda BT}{\rho})\boldsymbol{ln}\varepsilon_\lambda\}]} \quad (7)$$

Where, BT is at- sensor BT in Celsius (C◦), λ is the mean wavelength of band 10 or 11, ελ is the emissivity calculated from equation 5 and ρ is $(\boldsymbol{h}\, \boldsymbol{x} \frac{\boldsymbol{c}}{\boldsymbol{\sigma}})$ which is = 1.438 x 10-2 mk in which, σ is the Boltzmann constant = 1.38 x 10-23 J/K, h is Plank constant = 6.626 x 10-34 and c is the velocity of light = 3 x 108 m/s.

4. Results

Two LANDSAT-8 images were acquired. One image was obtained on March the 2nd, 2013; the other image was obtained on March the 18th, 2013 and both were used in this paper. The land cover was classified into four types on cloud-free LANDSAT-8 image which was acquired on the 02/03/2018 and ten types on cloud-free LANDSAT-8 image which was acquired on 18/03/2018. The two images were taken at the same time the ground-truth field was measured with a direct connection with land surface, as shown consecutively on tables 5 and 6. Were taken at the same time the ground-truth field was measured with a direct connection with land surface, as shown consecutively on tables 5 and 6. As shown in Table 5 the difference between the IR thermometer camera measurements (type-k) and LST retrieved ranges between 0.4 C◦ and 1.77 C◦ with the correlation coefficient of the two bands 10 and 11 R_{bnad10}= 0.70, R_{band11} = 0.89 respectively.

The results shown are satisfactory and this is due to the less measurement undertaken and the scene center time recorded which was in 10:33:42 local time according to Metadata. On the other hand Table 6 shows an extraordinary results between the IR thermometer camera measurements (type-k) and the LST retrieved measurements R_{band10} =0.70 and R_{band11} = 0.72, the errors ranges between -0.02 C◦ and 3.47 C◦. The results reveal that there is a high error in water (3.47 C◦) and less errors in vegetation which ranges between -0.02 C◦ – 1 C◦

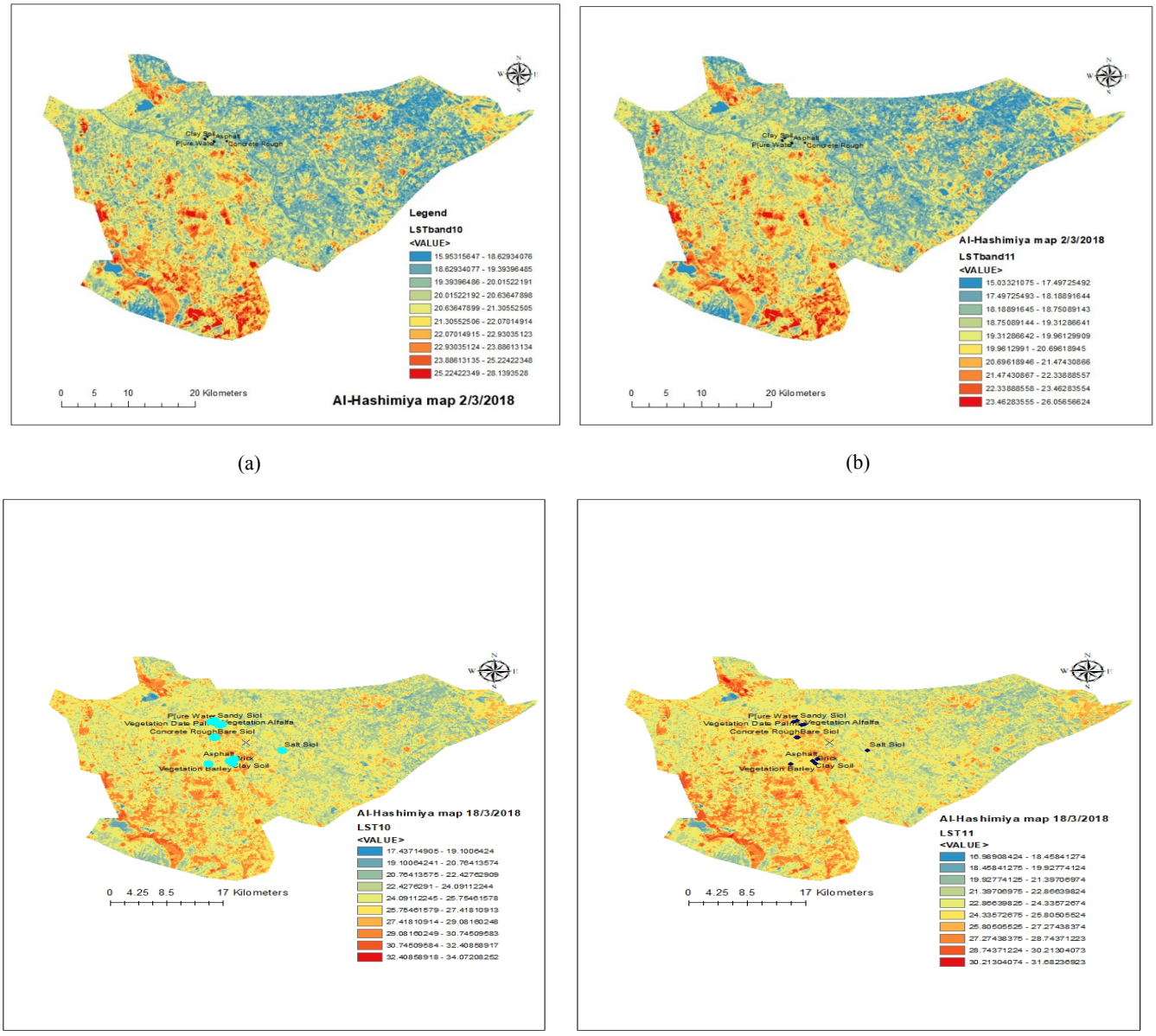

(a) (b)

(c) (d)

Fig. 6: LST of Al-Hashimiya (a) and (b) LST maps of the two bands 10 and 11 respectively image acquired on 2-3-2018, (c) and (d) LST maps of the two bands 10 and 11 respectively image acquired on 18-3-2018.

Table. 5: Retrieved LST and IR thermometer camera for TIRS bands 10 and 11 for 02/03/2018

Time of measured Am	Latitude	Longitude	Land cover types	Land cover class	02/03/2018 band 10			02/03/2018 band 11		
					LST Retrieved (C◦)	Type-k thermometer camera (C◦)	Error (C◦)	LST Retrieved (C◦)	Type-thermometer camera (C◦)	Error (C◦)
9:45	467483	3582422	Water	River	18.77	17.00	1.77	18.64	17.0	1.64
10:00	467554	3582366	Soil	Clay soil	19.86	18.20	1.66	18.60	18.20	0.40
10:45	468906	3581914	Vegetation	Alfalfa	19.99	21.40	-1.41	19.75	21.40	-1.65
10:30	468886	3581957	Building	Asphalt	19.86	19.2	0.66	18.68	19.20	-0.52

The errors in vegetation recorded were due to a close scene center time (10:33:34) acquired compared to the measurements of the buildings, soil and water. However the least errors shown in Table 5 were recorded in soil and buildings that ranges between -0.52 C◦ – 0.4 C◦. Generally the results show that the closer measurement taken from the scene center time, a better quality to classify the land cover

Table 6: Retrieved LST and IR thermometer camera for TIRS bands 10 and 11 for18/03/2018

Time of measured Am	Latitude	Longitude	Land cover types	Land cover class	18/03/2018 band 10			18/03/2018 band 11		
					LST Retrieved (C◦)	Type-k thermometer camera (C◦)	Error (C◦)	LST Retrieved (C◦)	Type-k thermometer camera (C◦)	Error (C◦)
10:15	467659	3582611	water	River	24.27	20.80	3.47	23.19	20.80	2.39
9:45	470449	3574270	soil	Clay soil	25.34	23.10	2.24	24.13	23.10	1.03
10:20	468194	3582870	Soil	Sandy soil	23.50	24.7	-1.2	22.58	24.70	-2.12

10:00	468300	3579318	Soil	Bare soil	28.48	28.6	-0.12	26.94	28.6	-1.66
10:20	467251	3573651	Vegetation	Barley	24.86	23.00	1.86	24.02	23.00	1.02
10:33	469203	3582082	Vegetation	Date Palms	24.97	24.3	0.67	24.03	24.3	-0.27
10:30	468897	3581936	Vegetation	Alfalfa	24.80	23.9	0.90	23.88	23.9	-0.02
10:05	468118	3579330	Building	Concrete	28.31	27.6	0.71	26.82-0.78	27.6	-0.78
11:00	470819	3573715	Building	Brick	25.55	25.10	0.45	24.34	25.10	-0.76
9:51	471153	3574666	Building	Asphalt	28.21	25.6	2.61	26.74	25.6	1.14

5. Conclusions

The algorithm created in the ArcGis, to estimate the LST for the selected datasets with direct contact with the study area. the proposed algorithm was created using the brightness temperature of thermal infrared of two bands 10 and 11 and emissivity of different land cover types, obtained from visible and near infrared bands of LANDSAT-8.the estimated LSTs were verified using the infrared thermometer camera with contact directly with the land surface. By looking at the tables above, and by comparing the measurement results of the two images, the results obtained show that:

• The first image was gives high correlation coefficient of the two bands 10 and 11 Rbnad10= 0.70, Rband11 = 0.89 respectively, for the imaged acquired on the 2nd of march 2018 due to lack of measurements taken, in comparison with the second image whose correlation coefficient Rband10=0.70 and Rband11 = 0.72. The results showed a clear indication of the difference in measured temperature by IR thermometer camera and LST which showed the closer scene center time, the more accurate land cover classification.

• The errors in band 11 is always less than the errors occurring in band 10 in both images.

• The difference showed in the LST for the same class is due to the canopies (buildings or trees) that make a shadow on these classes.

References

[1] Lu D, Weng Q.," Spectral mixture analysis of ASTER images for examining the relationship between urban thermal features and biophysical descriptors in Indianapolis", *Remote Sensing of Environment*, Vol.104, No.2, (2006), pp.157-167.

[2] Weng Q, Lu D.," A sub-pixel analysis of urbanization effect on land surface temperature and its interplay with impervious surface and vegetation coverage in Indianapolis", *International Journal of Applied Earth Observation and Geoinformation,*Vol.10, No.1, (2008), pp.68-83.

[3] Patel N, Parida B, Venus V, Saha S, Dadhwal ," Analysis of agricultural drought using vegetation temperature condition index (VTCI) from Terra/MODIS satellite data", *Environmental Monitoring and Assessment*, Vol.184, NO.12, (2012), pp. 7153–7163.

[4] Krishna A P, Sharma A. s.l.," Snow cover and land surface temperature assessment of Gangotri basin in the Indian Himalayan Region (IHR) using MODIS satellite data for climate change inferences", *International Society for Optics and Photonics,* SPIE Remote Sensing, (2013), pp. 889314-889319.

[5] Karnieli, A., et al.," Use of NDVI and Land Surface Temperature for Drought Assessment", *American Meteorological Society*, Vol. 23, (2010), pp. 618-633.

[6] Kustas, W. and Anderson, M.," Advances in Thermal Infrared Remote Sensing for Land Surface Modeling. Kustas", *Agricultural and Forest Meteorology*, Vol.149, No.12, (2009), pp. 2071-2081.

[7] Agam, N., et al.," Utility of Thermal Image Sharpening for Monitoring Field-Scale Evapotranspiration Over Rainfed and Irrigated Agricultural Regions", *Geophysical Research Letters,* Vol.35, No.2, (2008), pp. L02402.

[8] C. Ottlé and D. Vidal-Madjar," Estimation of land surface temperature with NOAA9 data ", *Remote Sensing of Environment*, Vol.40, No.1, (21992), pp.27-41.

[9] L. M. Mcmillin," Estimation of sea surface temperatures from two infrared window measurements with different absorption", *J. Geophys.Res.*, Vol.80, No.36, (1975), pp. 5113-5117.

[10] Li, F. Becker and Z.-L.," Towards a local split window method over land surfaces", *International Journal of Remote Sensing,* VOL.11, NO.3, (1990), pp.369-393.

[11] Z. Wan and J. Dozier," A generalized split-window algorithm for retrieving land-surface temperature from space", *IEEE Transactions on Geoscience and Remote Sensing,* Vol.34, No.4, (1996), pp. 892 – 905.

[12] Z. Qin, G. Dall'Olmo, A. Karnieli, and P. Berliner," Derivation of split window algorithm and its sensitivity analysis for retrieving land surface temperature from NOAA-advanced very high resolution radiometer data", *J. Geophys.Res. Atmospheres,* Vol.106, NO.D19, (2001), pp. 22655-22670.

[13] Li, G.-M. Jiang and Z.-L," Split-window algorithm for land surface temperature estimation from MSG1-SEVIRI data", *International Journal of Remote Sensing,* Vol.29, No.20, (2008), pp. 6067-6074.

[14] G.-M. Jiang, W. Zhou, and R. Liu.," Development of split-window algorithm for land surface temperature estimation from the VIRR/FY-3A measurements", *IEEE Geoscience and Remote Sensing Letters,* Vol.10, No.4, (2013), pp. 952-956.

[15] G.-M. Jiang and R. Liu," Retrieval of sea and land surface temperature from SVISSR/FY-2C/D/E measurements", *IEEE Transactions on Geoscience and Remote Sensing,* Vol.52, No.10, (2014), pp. 6132 - 6140.

[16] Sobrino, G. Sòria and J. A.," ENVISAT/AATSR derived land surface temperature over a heterogeneous region", *Remote Sensing of Environment,* Vol.111, (2007), pp. 409-422.

[17] Rozenstein, Zhihao Qin, Yevgeny Derimian and Arnon Karnieli," Derivation of Land Surface Temperature for Landsat-8 TIRS Using a Split Window Algorithm", *Sensors Open Access Journal,* Vol.14, No.4, (2014), pp. 5768-5780.

[18] Internet-Website, (https://landsat.usgs.gov).

[19] Shanshan LI and Geng-Ming Jiang," Land Surface Temperature Retrieval from Landsat-8 Data with the Generalized Split-Window Algorithm", *IEEE Access,* Vol.6, (2018), pp. 18149 – 18162.

[20] IR Video Thermometer User Manual Model DT-9862.

[21] Walawender, J. p., Szymanowski, M., Hajto, M. J., Bokwa A.," Land syrface temperature patterns in the urban agglomeration of Krakow (Poland) mderived from Landsat-7/ETM+ data", *Pure and Applied Geophysics*, Vol.171, NO.6, (2014), pp. 913–940.

[22] Jose A. Sobrino, Juan C. Jimenez-Munoz, Guillem Sòria, Mireia Romaguera, Luis Guanter, Antonio Plaza, & Pablo Martínez," Land Surface Emissivity Retrieval from Different VNIR and TIR Sensors", *IEEE Transactions on Geoscience and Remote Sensing*, Vol.64, (2008), pp. 316 – 327.

[23] M. Stathopoulou, & C. Cartalis," Daytime urban heat islands from Landsat ETM+ and Corine land cover data: An application to major cities in Greece" , *Solar Energy*, Vol.81, No.3, (2007), pp. 358-368.